Alexandria Journal of Science and Technology

Article

Application of Remote Sensing and Structural Geology for Drainage Network Analysis and Environmental Hazard Assessment in East New Cairo – Egypt

El Nazeer H. Tawir[1,2,*], Tharwat A. Abdel Fattah[2], Magdy MS. El Maghraby[2], Manal M. Osman[2], Ahmed M. Lithy[3], Abbas M. Abbas[3]

[1] *Geology Department, Faculty of Science, University of Kordofan, El-Obied, Sudan.*

[2] *Geology Department, Faculty of Science, Alexandria University, Alexandria, Egypt.*

[3] *National Research Institute of Astronomy and Geophysics, Helwan, Cairo.*

[*] *Correspondence Address:*

El Nazeer H. Tawir: Geology Department, Faculty of Science, University of Kordofan, El-Obied, Sudan, E-mail address: elnazeerh@gmail.com.

KEYWORDS: Regional Slope; Flow direction; Flash flooding; Digital elevation model (DEM); Predicted Faults.

Received:
December 12, 2024
Accepted:
March 03, 2025
Published:
March 28, 2025

ABSTRACT: This study analyzes drainage network systems in East New Cairo, Egypt. It uses high-resolution satellite imagery and DEM-derived data to assess environmental hazards, map structural features, and correlate them with drainage networks. Through Digital Elevation Model (DEM) analysis and hill-shaded relief imaging, we identified drainage patterns and their intensity across the region. The extracted drainage network revealed a complex system characterized by trellis and radial patterns, comprising five stream orders of varying lengths. Areas with high drainage density, particularly in the eastern part of the study area, raise significant concerns about potential subsurface infiltration and future soil condition alterations. However, the overall drainage suggests minimal surface flooding risk. Notably, rather than tectonic activity, regional slopes are the primary determinant of drainage patterns and fault orientations. A critical finding is an impermeable clay layer near the surface, which may cause water accumulation and rising water levels. Exacerbated by excessive irrigation, this shallow impermeable layer prevents water penetration into deeper soil strata, potentially creating substantial construction challenges. By correlating field-mapped structures with DEM-derived drainage patterns, the research identified 22 normal faults influencing the drainage network, several of which were confirmed through rigorous field observations. These findings provide crucial insights into the region's structural geology by identifying new fault geometries and their interactions with hydrological systems. These offer valuable perspectives for managing environmental risks associated with fault activity and soil instability.

1. INTRODCTION

The study and analysis of drainage networks have received significant attention across various disciplines due to their environmental and geological impacts. Drainage networks play a vital role in understanding groundwater flow and accumulation [1, 2, 3, 4, 5], assessing environmental hazards such as flash floods [6, 7, 8, 9], and analyzing fault initiation and development associated with tectonic processes [10].

Drainage systems and stream networks also contribute to sediment transport, erosion, and deposition. Eroded materials carried by surface water tend to accumulate in floodplains, significantly shaping the landscape [11, 12].

Drainage patterns, categorized as trellis, dendritic, rectangular, parallel, radial, contorted, or annular (**Figure 1**), are influenced by regional slope, lithology, rock hardness, climate, and tectonic activity [13]

Alexandria Journal of Science and Technology, 2025, **3**(1), 53–61
Online ISSN: 2974-3273

DOI: 10.21608/AJST.2025.343324.1056

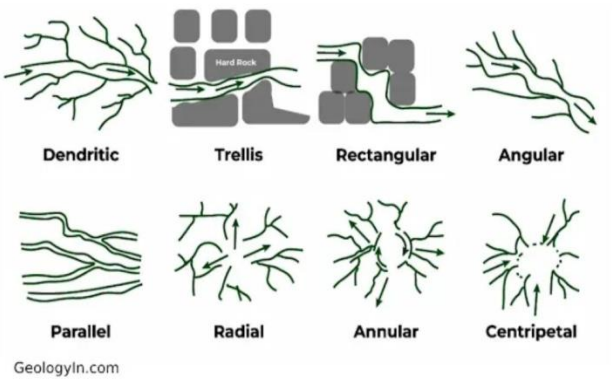

Figure 1. Types of Drainage Patterns [13].

Geological structures, including faults and fractures, often have a profound effect on drainage formation. Variations in lithology and tectonic settings can alter typical patterns, resulting in structural modifications [14, 15, 16].

The relationship between geologic structures and drainage patterns is well-documented [17, 18, 19, 20, 21]. Features such as faults, fractures, fold axes, and dipping sedimentary layers influence flow direction, leading to alignment between drainage networks and subsurface geology. In tectonically active basins, structural features critically shape drainage patterns, as seen with relay ramps impacting drainage and sedimentation [22].

Recent advancements in remote sensing, with improved spectral and spatial resolution, have facilitated detailed mapping of drainage patterns, terrain, and geologic structures. Combined with Geographic Information Systems (GIS), these technologies enable efficient data collection, analysis, and presentation for geological research [23, 24, 25, 26, 27]. This integration has proven invaluable for mapping faults and drainage systems, significantly enhancing our understanding of geological processes [19].

This study leverages these technological advancements to explore the relationship between fault types, structural geometries, and drainage patterns in the study area. By integrating field mapping, high-resolution satellite imagery, and Digital Elevation Models (DEMs) analyzed within a GIS framework, the research aims to provide a detailed understanding of the region while assessing risks related to faults and flooding.

2. Geology Settings

2.1. Study Area

The study area lies within New Cairo, established in 2000, covering approximately 250 km². Designed to accommodate a population of four million people [28], New Cairo features diverse land uses, including residential, commercial, industrial, and service sectors.

Located northeast of New Cairo City and south of the Cairo-Suez Road, the area is bordered by the Ring Road to the west, Gebel El-Anqaabiya Road to the east, the Cairo-Suez desert route to the north, and the El-Qattamiya-Ain El-Sokhna Road to the south (**Figure 2**). The region exhibits significant topographical variation, with elevations ranging from 420 meters above mean sea level (AMSL) at the southeastern boundary to 142 meters AMSL in the northwestern part [28]. The area is characterized by isolated low hills, darker ridges aligned in WNW-ESE and E-W directions, and elevations of 150 to 200 meters. In the northern part, a broad plain extends northward and northwestward, drained by numerous watercourses originating from the south, southwest, and southeast (**Figure 3**).

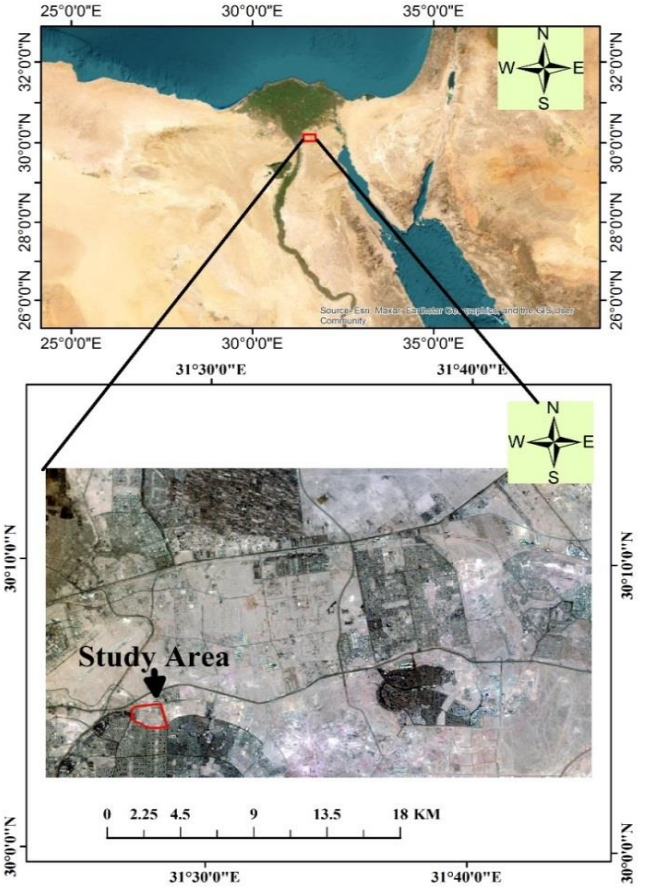

Figure 2. Location of the Study Area.

2.2. Geology and Geomorphology

The region between the Cairo - Suez and El-Sukhna-Qattamiya districts is characterized by sedimentary rocks and basaltic flows formations. Studies by [29] and [30], indicate that these rocks range in age from the Middle Eocene (Mokattam Formation) to the Middle Miocene (Hommath Formation), with Eocene layers unconformably overlying Upper Cretaceous beds.

Prominent in the area east of Cairo are Oligocene rocks, particularly between the Cairo-Suez and Qattamiya-El Sukhna districts. The Oligocene sequence consists of loosely packed sands and gravels, known as the Gebel Ahmer Formation, overlying basaltic sheets. The Gebel Ahmer Formation features cross-bedded, medium- to coarse-grained sandstones in various colors, interspersed with thin gravel beds and lenses. These deposits often contain pebble-sized flint and silicified wood fragments. While the sands and gravels are generally poorly

cemented, fracture zones exhibit enhanced cementation from silica and iron-rich solutions.

Miocene deposits typically overlie Oligocene rocks and are divided into two distinct units:

- Marine sediments (Hommath Formation) at the base.
- Non-marine sediments (Hagul Formation) above, separated by an unconformity [31].

The Oligocene sediments are primarily located in structural depressions bordered by northwest-trending faults [32]. In contrast, the Paleogene sequence of East Cairo formed within an E-W oriented graben system, a down-dropped crustal block bounded by parallel faults. Additional fault systems in the area trend E-W to WNW-ESE (**Figure 4**).

During the Late Eocene, the region experienced an initial phase of NE-SW extension, followed by a second extension phase during the Late Oligocene and Miocene. This later phase was associated with the regional extension tied to the opening of the Gulf of Suez rift, which was also marked by basaltic eruptions. Oligocene rocks were subsequently cut by NW-SE-striking faults, suggesting fault reactivation post-deposition [33].

The Cairo-Suez Province, functioning as a significant transfer zone, exhibited E-W elongated belts of left-stepped en echelon NW-SE, WNW-ESE, and E-W striking normal faults. These belts were often accompanied by en echelon faults striking NW, reflecting the tectonic complexity of the region [33].

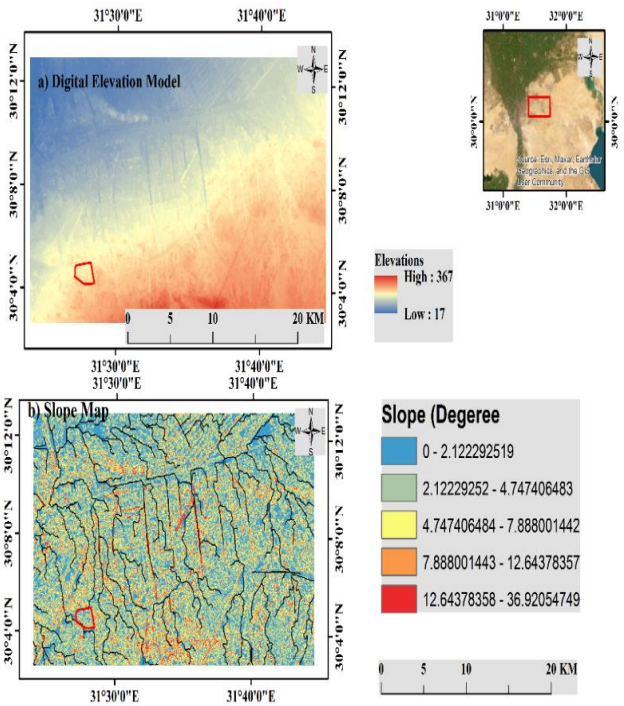

Figure 3. ASTER (DEM) for the study area showing the variation in Topography: (a) (DEM) map and (b) Slope map.

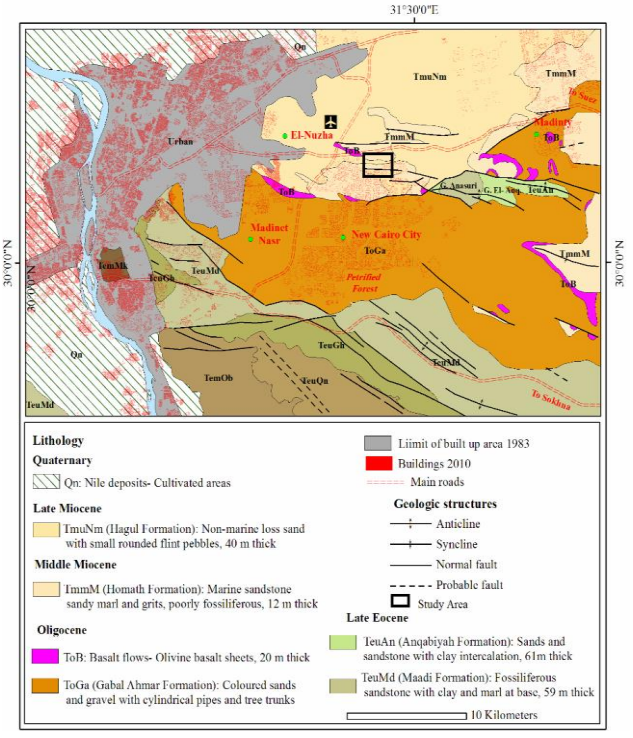

Figure 4. Geological Map of Greater Cairo (Modified after the Egyptian Geological Survey and Mining 1983).

The study area is located within the Cairo-Suez Province (CSP), which stretches from the eastern part of the Nile fluvial plain to the west of the Suez Canal and the northern portion of the Gulf of Suez (**Figure 5**). The elevation in the CSP gradually decreases toward the north, with the highest elevations and steepest slopes in the southern part of the province. For instance, the altitude in the southern region reaches up to 850 meters above sea level, such as at G. Ataqa on the eastern side of the CSP (**Figure 5**). In contrast, the northern area is predominantly flat, with about 70% of the landmass located at elevations of approximately 150 meters above sea level [34]. However, some localized hilly scarps, such as G. Eweibed (~400 meters) and G. Gafra (~200 meters), can be found (**Figure 5**). The regional slope ranges from 0° to 68°, and the climate in the study area is predominantly arid to semi-arid, with an average annual precipitation of about 70 mm.

The southern part of the region is characterized by dissected, high-elevation mountains, separated by distinct drainage patterns and interfluves. In contrast, the northern part of the region features more widespread, dendritic drainage patterns due to its flat, gently sloping topography. Wadi Gafra (**Figure 5**) is the most prominent in the northern region, exhibiting a dense dendritic network of tributaries that expand in width depending on the slope and rock permeability. Wadi Ghoweiba and Wadi Hagul (**Figure 5**) are large, extended wadis in the southern CSP. The main wadis in the area are structurally controlled, with their courses following major faults, while the tributaries are influenced by lithological fractures and/or regional slope variations.

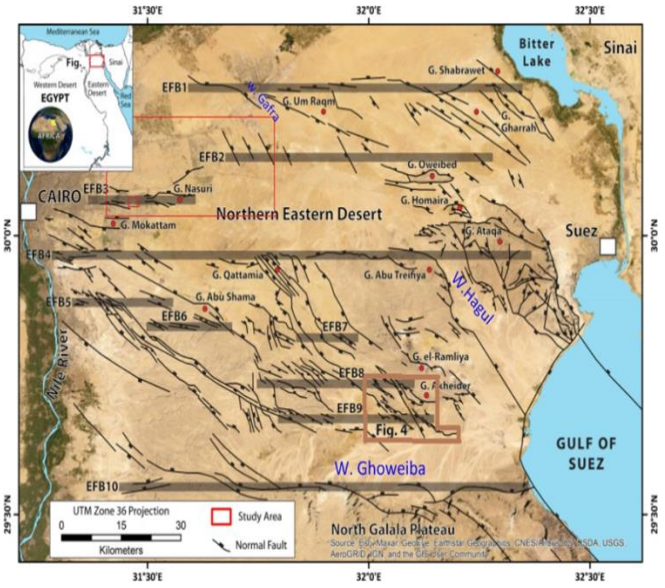

Figure 5. Detailed structural map of the Cairo-Suez Province, northern Eastern Desert of Egypt, showing the location of the present study area [33].

3. Methodology

3.1. Remote Sensing Data

Active remote sensing data, particularly radar sensors, is widely recognized as an effective technology for mapping drainage networks and identifying geological structures [35, 36, 37]. We used data from the Advanced Spaceborne Thermal Emission and Reflection Radiometer (ASTER), which is known for its ability to provide detailed elevation data. The data, provided by the National Aeronautics and Space Administration (NASA) and the National Geospatial-Intelligence Agency (NGA), offers near-global coverage and generates high-resolution topographic maps of the Earth's surface. For our study area, we obtained four ASTERGL images with a spatial resolution of 30 meters, along with two Landsat images (OLI/TIRS), which were sourced from the US Geological Survey (USGS) website (http://earthexplorer.usgs.gov), [38]. All the images were georeferenced to the Universal Transverse Mercator (UTM, WGS, zone 36 N). Information on the satellite images used in this research is provided in (Table 1).

3.2. Geospatial Data Preparation

Our approach to preparing geospatial data is meticulous, involving several steps such as co-registration, data manipulation, clipping, mosaicking, and storage.

Table 1: Information about the satellite images used in this research.

Data obtained	Spacecraft/Sensor	Path/Row	Pixel Size (m)	Coordinate System/Datum	Zone
2013-04-29	LANDSAT-8/ OLI	176/39	30	UTM/WGS 84	36
2022-08-04	LANDSAT-9/ OLI, TIRS	176/39	15	UTM/WGS 84	36

The ASTER Digital Elevation Model (DEM) data, a crucial component in our research due to its high spatial resolution and global coverage, was processed using ArcGIS 10.5 software. This data, which provides detailed information about the Earth's surface, was used to derive elevation zones, slope angles, and stream networks, forming the rigorous basis of our analysis.

Many GIS spatial analysis tools were employed to support the objectives of the research:

a. The ASTER images were combined using the ArcGIS "Mosaic to New Raster" tool and clipped to focus on the area.
b. The drainage pattern was delineated by analyzing the clipped ASTER images using ArcGIS hydro tools. This involved several steps: Fill Sink, Flow Direction, Accumulation, Stream Definition, Segmentation, and the final Drainage Line Processing task to create the stream network.
c. The flow direction image was then used to analyze the relationship between the stream network's flow paths and the study area's regional slope and structural features.
d. The clipped images were relief-shaded using the ArcGIS Hillshade Analyst tool, a process that provided a clear and insightful view of the terrain. This approach not only enhances the interpretability of our results but also allows for the visual identification of structural features, providing a clear and detailed view of the terrain that is easily interpretable.

Figure 6 outlines the process used to analyze the study area's geomorphological features, which involved a detailed analysis of the ASTER DEM data using a series of spatial analysis tools and techniques.

This study utilized two Landsat images (path/row: 176/39), specifically from the Operational Land Imager/Thermal Infrared Sensor (OLI/TIRS), acquired on April 29, 2013, and August 4, 2022. The OLI sensor includes 11 spectral bands, covering wavelengths from the blue to shortwave infrared (SWIR) range (Table 2). These bands include multispectral bands with a spatial resolution of 30 meters for visible and near-infrared light and a panchromatic band with a higher spatial resolution of 15 meters.

The following flow chart (**Figure 6**) illustrates the steps of perform remote sensing methodology.

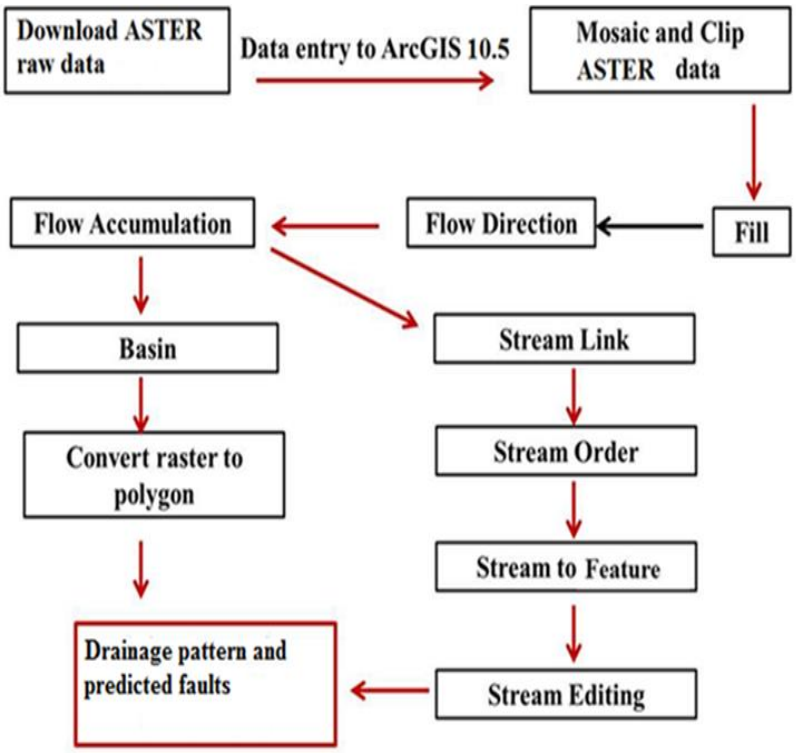

Figure 6. Flowchart of the process of ASTER DEM analysis.

Table 2: Operational Land Imager (OLI) spectral bands [39].

#	Band	Minimum lower band edge (nm)	Maximum Upper Band edge (nm)	Center Wavelength(nm)	Maximum Spatial Resolution At Nadir(m)
1	Coastal/Aerosol	433	453	443	30
2	Blue	450	515	482	30
3	Green	525	600	562	30
4	Red	630	680	655	30
5	NIR	845	885	865	30
6	SWIR1	1560	1660	1610	30
7	SWIR2	2100	2300	2200	30
8	Panchromatic	500	680	590	15
9	Cirrus	1360	1390	1375	30
10	Thermal	10300	11300	10800	100
11	Thermal	11500	12500	12000	100

4. Results and Discussion

This analysis plays a crucial role in multiple geological and environmental domains, including comprehensive environmental hazard assessment. Moreover, changes in terrain texture and pattern can also help in extracting information about weak zones in the surface layers and rock. types. The hill-shaded relief images (**Figures 7**) significantly enhance the visibility of linear and curvilinear features, effectively revealing potential fault structures and providing critical insights into the surface geological structure

framework. The extracted drainage pattern reveals the presence of both trellis and radial patterns across the study area. These patterns have direct implications for construction activities, as the drainage networks could lead to localized flooding. (**Figure 8**) illustrates the distribution and hierarchy of streams within the study area, which includes five stream orders of varying lengths. Notably, the oldest network, a fifth-order stream, is located in the northwest section. The majority of streams are situated peripherally, with only a small first-order stream traversing the study area's boundaries. These observations indicate a low probability of significant surface flooding risks. Nevertheless, the elevated drainage density in the eastern sector presents potential concerns regarding surface water infiltration into subsurface layers, which may progressively compromise soil structural integrity and geological stability.

In several instances, the branches of the drainage pattern and faults exhibit differing orientations, indicating that regional slopes, rather than tectonic forces, predominantly influence these features. This distinction is essential for understanding the geological processes shaping the drainage network and their implications for land use planning and hazard mitigation.

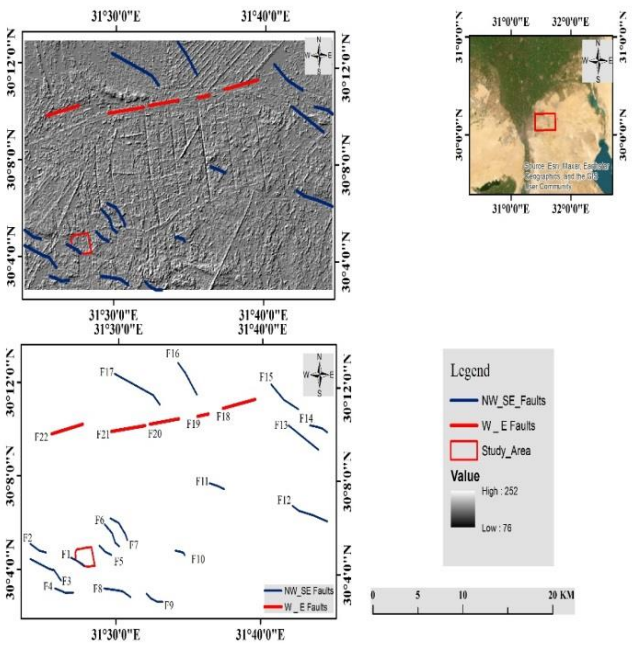

Figure 7. Extracted predicted faults with the mapped structures overlaid on hill shaded ASTER DEM image.

The higher drainage density in the eastern part of the study area, highlighted by the black box in (**Figure 9**), indicates faster water movement, which can increase soil saturation in this region. Water is likely to accumulate just above the shallow clay layer, which acts as an impermeable barrier. This layer's low permeability could cause water to rise to the surface, potentially leading to complications for future construction projects (**Figure 10**).

Excessive surface irrigation significantly compounds this hydrological challenge by introducing substantial water volumes into subsurface layers. However, the presence of an impermeable clay layer at shallow depths critically inhibits water infiltration into deeper geological strata. Field observations (**Figure 10**) definitively confirmed the existence of a water-saturated layer positioned immediately above the impermeable clay substrate, creating a distinct hydraulic barrier. This geological configuration fundamentally restricts further water penetration, underscoring the critical importance of advanced water management and strategic construction planning in the region.

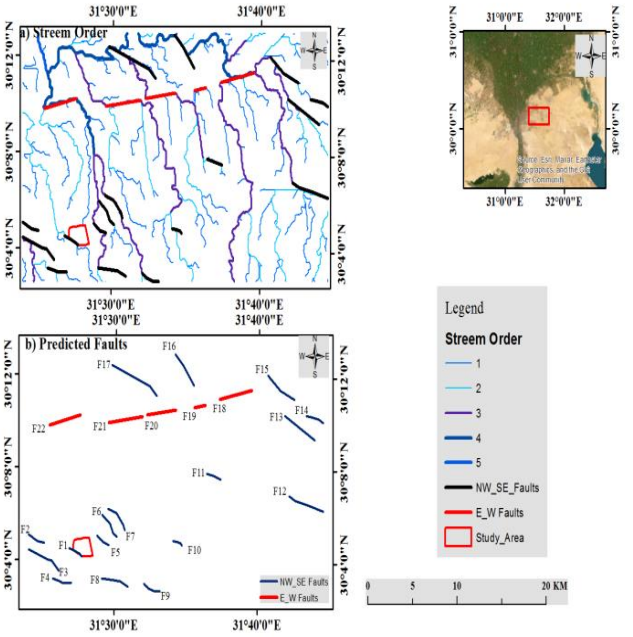

Figure 8. Extracted drainage network from ASTERDEM with the mapped, (a) Stream order, (b) Predicted Faults.

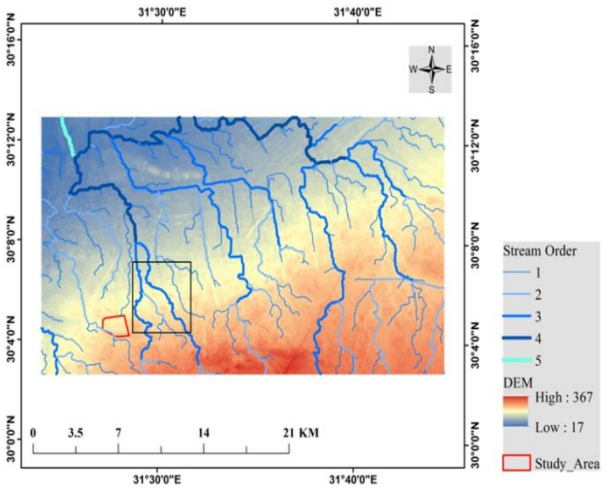

Figure 9. Show drainage density around the study area (black box).

Numerous case studies highlight the significant impact of drainage density on clay layers in East Cairo. In rapidly urbanizing areas such as New Cairo and Nasr City (**Figure 11**), changes to the drainage network have directly influenced the stability of clay soils. The increased drainage density, combined with the expansion of impermeable surfaces, has exacerbated foundation issues in these regions. These challenges primarily arise from the presence of the underlying impermeable clay layer, which restricts water infiltration and impacts soil stability.

Figure 10. The area of swamps is being formed by seepage water.

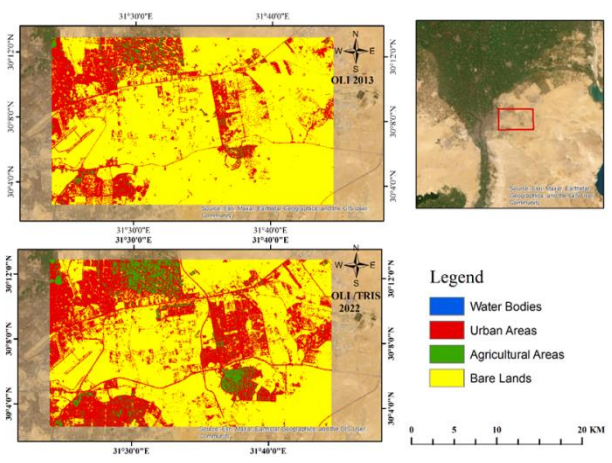

Figure 11. Supervised classification for the study area appears different classes and urban distribution.

4.1 Predicted Faults

This analysis highlights the integral role of structural features, particularly faults, in shaping the drainage pattern of the study area. By leveraging field data, high-resolution satellite imagery, and DEM-derived drainage networks, the research identified 22 fault-related structural geometries that influence drainage. The confirmation of specific faults through both field surveys and prior geological studies underscores the robustness of the findings. As a result, the following findings are concluded.

1. **Predominance of NW-SE Oriented Faults**:

- Faults such as F1, F3, F5, F9, F10, and F14 exhibit a NW-SE orientation (**Figure 12 b**).
- This orientation aligns with consistent trends noted in previous studies, indicating a well-documented regional structural direction.

2. **Presence of W-E Oriented Faults**:

- Five faults (marked in yellow in **Figure 12 b**) with a E-W orientation were also validated by earlier geological investigations.
- This secondary trend refines the understanding of structural variability within the region.

3. **Methodological Correlation**:

- The integration of field-mapped structures, satellite imagery, and DEM-based drainage patterns provided a comprehensive framework for fault identification.
- The ability to confirm faults like F1 and F5 through field surveys demonstrates the reliability of the methodological approach.

4. **Regional Structural Framework Refinement**

- The study's findings not only corroborate past geological research but also enhance the existing structural model by identifying additional fault geometries.

These insights collectively enhance the understanding of the interplay between structural geology and hydrology in the area, offering a refined perspective on regional tectonics and their influence on surface processes. The detailed correlation of faults with drainage patterns has significant implications for future geological, hydrological, and geotechnical studies.

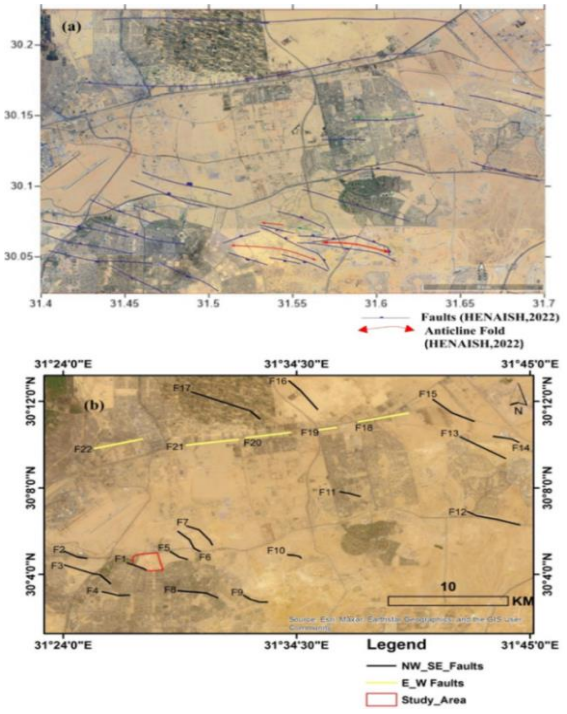

Figure 12. Major structural features (i.e. faults) affected on study area. (a) Structural map modified by [34], (b) predicted Fault extracted from Drainage pattern.

5. Conclusion

The integration of field surveys, high-resolution satellite imagery, and DEM-derived data demonstrated a robust methodology, enabling precise mapping of structural features and their correlation with drainage networks. The research systematically delineates 22 normal faults that critically influence the drainage network's configuration. Two predominant fault orientations were identified: Northwest-Southeast oriented faults (including F1, F3, F5, F9, F10, and F14) and West-East oriented faults (comprising F2, F4, F6, F8, and F12). These structural configurations provide essential insights for geotechnical assessment and strategic site selection in construction planning. Areas with high drainage density, particularly in the eastern part of the study area, pose risks of soil saturation above impermeable clay layers. This highlights the necessity of implementing effective water management strategies and careful construction planning to mitigate challenges related to soil instability and surface water retention.

The findings enhance the understanding of the region's structural geology by identifying new fault geometries and their interactions with hydrological systems. These insights are crucial for hazard mitigation, land use planning, and further geological studies, offering a more refined perspective on regional tectonics.

Other validation criteria should be recommended to interpret anomalous drainage network offsets with faulting. These include Topographic and Geomorphic Analysis, Geological Mapping and lithology, and Hydrological and Fluvial Processes.

6. Acknowledgment

We extend our sincere gratitude to the numerous individuals and institutions whose invaluable support and contributions were instrumental in the development and successful completion of this research endeavor. Special thanks are due to our colleagues, research assistants, and the technical staff who provided critical insights, logistical support, and expert guidance throughout the various stages of this scientific investigation.

References

[1] Hunt, B. B.; Smith, B. A.; Andrews, A.; Wierman, D. A.; Broun, A. S.; Gary, M. O. Relay Ramp Structures and Their Influence on Groundwater Flow in the Edwards and Trinity Aquifers, Hays and Travis Counties, Central Texas. SiHo Con. 2015, 189, 200.

[2] Jesiya, N. P.; Gopinath, G. A. Fuzzy-Based MCDM–GIS Framework to Evaluate Groundwater Potential Index for Sustainable Groundwater Management - A Case Study in an Urban-Periurban Ensemble, Southern India. Groundw. Sustain. Dev. 2020, 100466.

[3] Ahmed, A.; Alrajhi, A.; Alquwaizany, A. S. Identification of Groundwater Potential Recharge Zones in Flinders Ranges, South Australia Using Remote Sensing, GIS, and MIF Techniques. Water 2021, 13, 2571.

[4] Mseli, Z. H.; Mwegoha, W. J.; Gaduputi, S. Identification of Potential Groundwater Recharge Zones at Makutupora Basin, Dodoma Tanzania. Geo. Eco. Landscapes 2023, 7, 198-211.

[5] Ndhlovu, G. Z.; Woyessa, Y. E. Integrated Assessment of Groundwater Potential Using Geospatial Techniques in Southern Africa: A Case Study in the Zambezi River Basin. Water 2021, 13, 2610.

[6] Alam, A.; Ahmed, B.; Sammonds, P. Flash Flood Susceptibility Assessment Using the Parameters of Drainage Basin Morphometry in SE Bangladesh. Quat. Int. 2021, 575, 295-307.

[7] Prama, M.; Omran, A.; Schröder, D.; Abouelmagd, A. Vulnerability Assessment of Flash Floods in Wadi Dahab Basin, Egypt. Environ. Earth Sci. 2020, 114, 1-17.

[8] Hassan, A.; Albanai, J. A.; Goudie, A. Modeling and Managing Flash Flood Hazards in the State of Kuwait: A Hydrogeomorphological Study. Hydroclimatic Extremes in the Middle East and North Africa, Elsevier, 2024, 129-147.

[9] Kruczkiewicz, A.; Bucherie, A.; Ayala, F.; Hultquist, C.; Vergara, H.; Mason, S.; Bazo, J.; de Sherbinin, A. Development of a Flash Flood Confidence Index from Disaster Reports and Geophysical Susceptibility. Remote Sens. 2021, 13, 2764.

[10] Giaconia, F.; Booth-Rea, G. G.; Martínez-Martínez, J. M.; Azañón, J. M.; Pérez-Romero, J. J.; Villegas, I. Mountain Front Migration and Drainage Captures Related to Fault Segment Linkage and Growth: The Polopos Transpressive Fault Zone (Southeastern Betics, SE Spain). J. Struct. Geol. 2013, 46, 76-91.

[11] Athmer, W.; Luthi, S. M. The Effect of Relay Ramps on Sediment Routes and Deposition: A Review. Sediment. Geol. 2011, 242, 1-17.

[12] Earle, S. Physical Geology, 2nd ed.; BC Campus: Victoria, B.C., 2019.

[13] Howard, A. D. Drainage Analysis in Geological Interpretation: A Summation. AAPG Bull. 1967, 51, 2246–2259.

[14] Deffontaines, B.; Lacombe, O.; Angelier, J.; Chu, H. T.; Mouthereau, F.; Lee, C. T.; Deramond, J.; Lee, J. F.; Yu, M. S.; Liew, P. M. Quaternary Transfer Faulting in the Taiwan Foothills: Evidence from a Multisource Approach. Tectonophysics 1997, 274, 61–82.

[15] Ali, U.; Ali, S. A. Investigation of drainage for structures, lithology and priority (Flood and Landslide) assessment using geospatial technology, J&K, NW Himalaya. In: Singh, V., et al., eds. Hydrologic Modeling. Singapore, 2018; pp. 135-160.

[16] Pubellier, M.; Deffontaines, B.; Quebral, R.; Rangin, C. Drainage Network Analysis and

Tectonics of Mindanao, Southern Philippines. Geomorphology 1994, 9, 325–342.

[17] Macka, Z. Structural Control on Drainage Network Orientation: An Example from the Loucka Drainage Basin, SE Margin of the Bohemian Massif (S Moravia, Czech Rep.). LFA 2003, 4, 109–117.

[18] Delcaillau, B.; Carozza, J. M.; Laville, E. Recent Fold Growth and Drainage Development: The Janauri and Chandigarh Anticlines in the Siwalik Foothills, Northwest India. Geomorphology 2006, 76, 241–256.

[19] Abdullah, A.; Nassr, S.; Ghaleeb, A. Remote Sensing and Geographic Information System for Fault Segments Mapping: A Study from Taiz Area, Yemen. J. Geo. Res. 2013, 201757.

[20] Odeh, T.; Gloaguen, R.; Mohammad, A. S. H.; Schirmer, M. Structural Control on Drainage Network and Catchment Area Geomorphology in the Dead Sea Area: An Evaluation Using Remote Sensing and Geographic Information Systems in the Wadi Zerka Ma'in Catchment Area (Jordan). Environ. Earth Sci. 2016, 75, 1–18.

[21] Wołosiewicz, B. The Influence of the Deep-Seated Geological Structures on the Landscape Morphology of the Dunajec River Catchment Area, Central Carpathians, Poland and Slovakia. Contemp. Trends Geosci. 2018, 7, 21–47.

[22] Moustafa, A. R.; Khalil, S. Control of Extensional Transfer Zones on Syntectonic and Posttectonic Sedimentation: Implications for Hydrocarbon Exploration. J. Geol. Soc., Ldn. 2017, 174, 318–335.

[23] Tlapáková, L.; Žaloudík, J.; Kulhavý, Z.; Pelíšek, I. Use of Remote Sensing for Identification and Description of Subsurface Drainage System Condition. Acta Univ. Agric. Silvic. Mendel. Brun. 2015, 63, 1587–1599.

[24] Singh, V.; Sinha, L. K.; Bhavani, A. G. Application of GIS and remote sensing technique in drainage network analysis: a case study of Naina–Gorma Basin of Rewa District, M.P., India. In: Rao, P., Rao, K., Kubo, S., eds. Remote Sensing for Disaster Management. Singapore, 2019; pp. 403–411.

[25] Attwa, M.; Henaish, A.; Zamzam, S. Hydrogeologic Characterization of a Fault-Related Dome Using Outcrop, Borehole, and Electrical Resistivity Data. Nat. Resour. Res. 2020, 29, 1143–1161.

[26] Jothimani, M.; Abebeb, A.; Duraisamy, R. Drainage Morphometric Analysis of Shope Watershed, Rift Valley, Ethiopia: Remote Sensing and GIS-Based Approach. Earth Environ. Sci. 2021, 796, 012009.

[27] Khalifa, A.; Bashir, B.; Çakir, Z.; Kaya, Ş.; Alsalman, A.; Henaish, A. Paradigm of Geological Mapping of the Adıyaman Fault Zone of Eastern Turkey Using Landsat 8 Remotely Sensed Data Coupled with PCA, ICA, and MNFA Techniques. ISPRS Int. J. Geo-Inf. 2021, 10, 368.

[28] Hassan, B. T.; Yassine, M.; Amin, D. Comparison of Urbanization, Climate Change, and Drainage Design Impacts on Urban Flash Floods in an Arid Region: Case Study New Cairo, Egypt. Water 2022, 14, 2430.

[29] Said, R. The Geology of Egypt; Elsevier: Amsterdam, New York, 1962.

[30] Abdel-Aal, M.E. Hydrogeological Evaluation of the Groundwater Resources in Cairo District [dissertation]; Ain Shams University: Cairo, 1982.

[31] Ismail, A. A.; Abdelghany, O. Lower Miocene Foraminifera from Some Exposures in the Cairo-Suez District, Eastern Desert, Egypt. J. Afr. Earth Sci. 1999, 28, 507–526.

[32] Moustafa, A. R. Structural Setting and Tectonic Evolution of North Sinai Folds, Egypt. Geol. Soc. Lond. 2010, 341, 37–63.

[33] Gamal, N.; Yousef, M.; Moustafa, A. R.; Bosworth, W. Spatiotemporal Evolution of Transfer Structures and Linked Fault Systems in an Extensional Setting. Southwest Gebel Akheider, Cairo-Suez District, Egypt. Mar. Pet. Geol. 2021, 133, 105260.

[34] Henaish, A.; Kharbish, S.; Zamzam, S. Structural Controls on Drainage Pattern Using Integration of Remote Sensing and Structural Data: Insights from Cairo-Suez Province, Egypt. CJEES 2022, 17, 131-142.

[35] Prabhakar, A. K.; Singh, K. K.; Lohani, A. K.; Chandniha, S. K. Study of Champua Watershed for Management of Resources by Using Morphometric Analysis and Satellite Imagery. Appl. Water Sci. 2019, 9, 127.

[36] Raju, S. R.; Raju, S. G.; Rajasekhar, M. Morphometric Analysis of Mandavi River Basin in Rayalaseema Region of Andhra Pradesh (South India), Using Remote Sensing and GIS. J. Ind. Geophys. Union. 2020, 24, 54-67.

[37] Abdelouhed, F.; Ahmed, A.; Abdellah, A.; Mohammed, I. Lineament Mapping in the Iknioun Area (Eastern Anti-Atlas, Morocco) Using Landsat-8 Oli and SRTM Data. Remote Sens. Appl., Soc. Environ. 2021, 23, 100606.

[38] USGS. Science for a Changing World. U.S. Department of the Interior U.S. Geological Survey. Available online: http://earthexplorer.usgs.gov (accessed on November 2022).

[39] Morfitt, R.; Barsi, J.; Levy, R.; Markham, B.; Micijevic, E.; Ong, L.; Vanderwerff, K. Landsat-8 Operational Land Imager (OLI) Radiometric Performance On-Orbit. Remote Sens. 2015, 7, 2208-2237.